ROYAL SOCIETY
OF CHEMISTRY

PAPER

Check for updates

An injectable ionic hydrogel inducing high temperature hyperthermia for microwave tumor ablation†

Jingyun Wang, [ab] Dan Wang, [ab] Hao Yan, [ab] Lei Tao, [c] Yen Wei, [c] Yongsan Li, [cd] Xing Wang, [d] Wei Zhao, [e] Yu Zhang, [f] Lingyun Zhao*[ab] and Xiaodan Sun*[ab]

Microwave tumor ablation is of clinical significance and has been considered as a promising cancer minimally invasive therapy. One of the challenges in this field is the optimization of the susceptible agent. Herein, a novel chitosan-based ionic hydrogel which can induce rather high temperature hyperthermia as a susceptible agent for microwave ablation is reported. Owning to the high porosity of the hydrogel, a strong ion confinement effect can be realized, therefore, strong polarization under microwave exposure is ensured for rapid heat generation. In addition, the as-synthesized hydrogel has negligible bio-toxicity and excellent spatial stability *in vivo* which can guarantee a reproducible therapeutic effect for repeated treatment. *In vivo* anti-tumor investigation has demonstrated that excellent therapeutic efficiency can be achieved after repeated microwave thermal therapy with a rather low power density (2.0 W, 2.45 GHz). Further, computer simulation was conducted to elucidate the microwave heating mechanism. Our investigation provides a biocompatible and stable agent for microwave tumor ablation and demonstrates its great significance for potential clinical application.

Introduction

Since the first use of percutaneous radiofrequency ablation for liver tumors in the 1990s,[1] thermal ablation of tumors has attracted tremendous attention in cancer therapy especially for the treatment of small, unresectable tumors or for patients who are poor surgical candidates. Compared with traditional surgical therapy, thermal ablation protocol offers several advantages such as lower morbidity, less damage to the surrounding tissues, reduced cost and shorter hospitalization time,[2] not to mention

[a] *State key laboratory of new ceramics and fine processing, School of Materials Science and Engineering, Tsinghua University, Beijing 100084, P. R. China. E-mail: sunxiaodan@mail.tsinghua.edu.cn*
[b] *Key Laboratory of Advanced Materials of Ministry of Education of China, School of Materials Science and Engineering, Tsinghua University, Beijing 100084, P. R. China*
[c] *Department of Chemistry, Center for Frontier Polymer Research, Tsinghua University, Beijing 100084, P. R. China*
[d] *Beijing Laboratory of Biomedical Materials, Beijing University of Chemical Technology, Beijing 100029, P. R. China*
[e] *Department of Interventional Radiology, Nanfang Hospital, Southern Medical University, Guangzhou 510515, Guangdong Province, China*
[f] *Guangdong Key Lab of Orthopedic Technology and Implant Materials, Key Laboratory of Trauma & Tissue Repair of Tropical Area of PLA, Guangzhou General Hospital of Guangzhou Military Command, Guangzhou 510010, China*
† Electronic supplementary information (ESI) available. See DOI: 10.1039/c7tb00556c

the ability to treat patients who are not candidates for conventional therapies in terms of clinic.[3]

Currently, radiofrequency ablation and microwave ablation are two commonly used thermal techniques, which are high temperature-based modalities (heating temperature > 60 °C).[4] In contrast to radiofrequency ablation, microwave ablation does not rely on electric currents and thus is more suitable for tissues with either higher impedance or a high water content, such as lungs, bone and tumors.[5] Moreover, it also has several unique advantages including faster intratumoral heat generation, larger tumor ablation volumes, deeper penetration in tissues, less susceptibility to different kinds of tissues and less procedural pain.[6–8] Therefore, microwave ablation has recently attracted a lot of interest in clinical oncology.[9,10] However, to the best of our knowledge, the microwave thermal dose is usually higher than 50 W, 2.45 GHz in clinical practice,[11–14] and the ablation temperature induced by microwave mainly relies on the water content of tissues, which still has the risk of overheating in surrounding healthy tissues. Therefore, a susceptible agent that has a high water content is indispensable in order to enhance the treatment efficiency and protect the healthy tissues.[15–19] Based on the electromagnetic energy heating mechanism that polar molecules attempt to continuously reorient in the oscillating electric field of electromagnetic radiation and therefore to generate heat by friction,[20] important properties for microwave ablation agents are relative permittivity and effective conductivity.[21]

Hence, materials with strong polarity which may be able to induce high temperature hyperthermia under microwave exposure can be selected as microwave susceptible agents to concentrate the heat and enhance the treatment efficiency.[22] Polyaniline (PANI) based composites, carbon fibers, rare earth compounds and magnetic iron oxide have been applied as microwave absorbers at high frequency (usually over 10 GHz) to improve the absorption efficiency in electromagnetic interference, environmental pollution, stealth technology in the military field, *etc.*[23–30] However, these materials are not suitable as microwave ablation agents because of their lower dielectric loss at the clinical microwave frequency (usually 2.45 GHz or 915 MHz). Polar materials such as ionic liquids, saline solution and saline microcapsules have been reported to enhance the microwave heating efficiency in tumor ablation.[9,10,31–36] Nevertheless, ionic liquids have high toxicity thus limiting their medical and biological applications, while saline solution and microcapsules have been reported to be rapidly cleared in human body and are not stable in repeated therapy sessions.[37,38] Therefore, more suitable non-toxic and spatial stable susceptible agent should be developed for microwave thermoablative technology applications. Hydrogels, due to their good tissue biocompatibility and solute permeability, are of great considerable interest as biomaterials and have been widely used for drug delivery, cell therapy, tissue engineering, *etc.*[39–47] They have been used to overcome the fast clearance deficiency, which offers a high-dose and constant release of drugs in the pathological tissues.[37,38,48,49] Their three-dimensional network is not only a nanoparticle carrier but also a good heat storage construction. Recent studies focusing on thermal effects have found that hydrogels can act as effective photothermal therapy (PTT) agents.[37,38] Here, heat was introduced not only to kill cancer cells, ease pain, and alleviate inflammation but also to make the hydrogel more biocompatible. Based on the above mentioned advantages of hydrogels, a scheme of the use of an injectable hydrogel for microwave tumor ablation was brought forward to achieve biocompatible and stable microwave thermal therapy.

Herein, we propose the application of a chitosan-based injectable ionic hydrogel inducing a high temperature rise for microwave tumor ablation. Chitosan is non-toxic, biodegradable and biocompatible, and thus bestows our hydrogel with excellent biocompatibility on. The injectability of the hydrogel was achieved by mixing a telechelic difunctional poly (ethylene glycol) (DF-PEG) solution and a glycol chitosan (CS) solution. Ions through saline were simply fixed in the hydrogel to achieve a strong ion confinement effect for further heat generation.[36,50] In addition, doxorubicin hydrochloride (DOX) was encapsulated within the hydrogel for combination chemotherapy. The simple but novel ionic hydrogel could be locally immobilized in tumors for a long time to induce repeated therapy sessions. Therefore, we demonstrated that this chitosan-based injectable ionic hydrogel could represent a promising vehicle for microwave ablation. The treatment process using this novel hydrogel is depicted in Fig. 1. The hydrogel induced a rapid and remarkable temperature increase *in vitro* from room temperature to 80 °C within 3 minutes. The susceptibility of the ionic hydrogel in a tissue-equivalent phantom model indicated that the ionic hydrogel could be significantly heated without causing overheating of the surrounding tissue under an ultralow microwave power (2.0 W, 2.45 GHz). Further *in vivo* anti-tumor investigation also demonstrated that excellent therapeutic efficiency can be achieved after repeated microwave thermal therapy with the same power (2.0 W, 2.45 GHz). The heating mechanism of the hydrogel
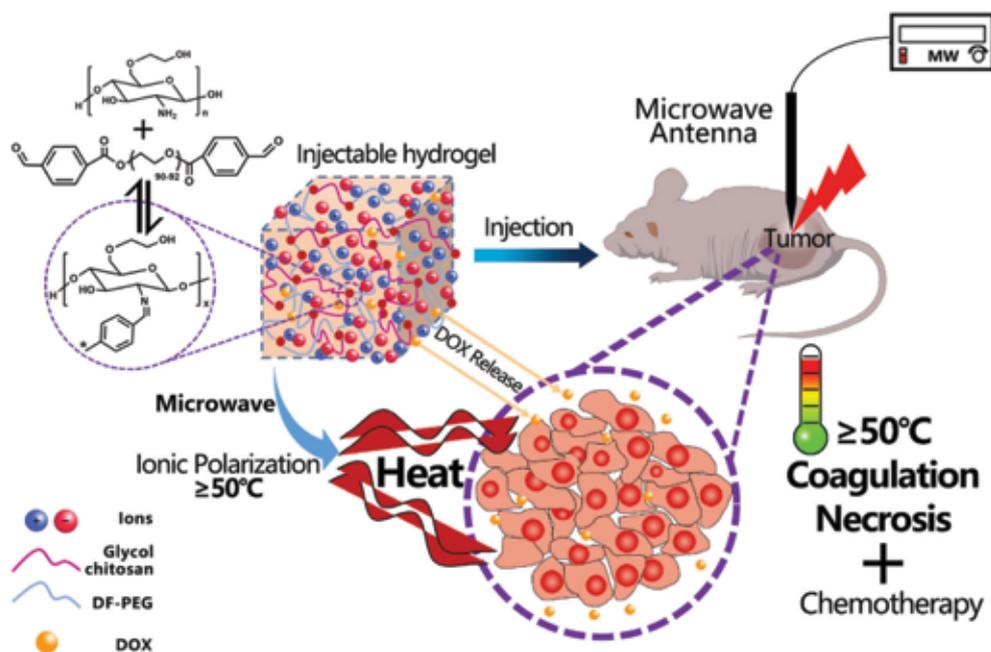
Fig. 1 Schematic illustration of microwave ablation therapy, including the chemical structure of the chitosan-based injectable ionic hydrogel. Benzaldehydes at both ends of difunctionalized PEG (DF-PEG) crosslinked with glycol chitosan as a functional group to form an injectable ionic hydrogel.

This journal is © The Royal Society of Chemistry 2017

J. Mater. Chem. B, 2017, **5**, 4110–4120 | **4111**

under microwave exposure was also explicated by evaluation *via* computer simulation using COMSOL 4.3b. This is the first trial to present an ionic hydrogel as a susceptible agent for microwave ablation therapy. The injectability and effectiveness of this novel chitosan-based ionic hydrogel confirm it as a promising candidate for microwave tumor ablation as well as for further clinical application.

Results and discussion

Characterization of the hydrogel

An injectable CS hydrogel with intrinsic self-healing capability was formed by a Schiff-base linkage (Fig. 1).[40] The reversible Schiff base (also known as imine, –N═CH–) linkage between NH_2 groups on CS and benzaldehyde groups at DF-PEG chain ends can be considered as a pseudocovalent linkage because of the intrinsic dynamic equilibrium between the Schiff base

bond and the aldehyde and amine reactants. A 0.3 cm hole in the center of the ionic hydrogel could finally disappear after 12 h by visual observation (Fig. 2a). This phenomenon illustrated the macroscopic self-healing properties of the ionic hydrogel. Quantitatively, rheology analysis was carried out. As shown in Fig. 2b (left), the storage modulus G' of the original ionic hydrogel remained stable at 1100 Pa with increasing frequency. When the ionic hydrogel was cut into 4 pieces, the time-dependent rheological test showed that G' dropped sharply because of the cutting damage (Fig. 2c). With increasing time, G' had an obvious rise until it reached the same level as that of the pristine hydrogel. The frequency-dependent rheological test was executed once again on this recovered hydrogel and almost the same mechanical behaviour as the original one was demonstrated, as shown in Fig. 2b (right). This process demonstrated that the ionic hydrogel has excellent self-healing property. To evaluate the strain-induced damage and healing of the hydrogel, a periodic step change of oscillatory strain between 300% and
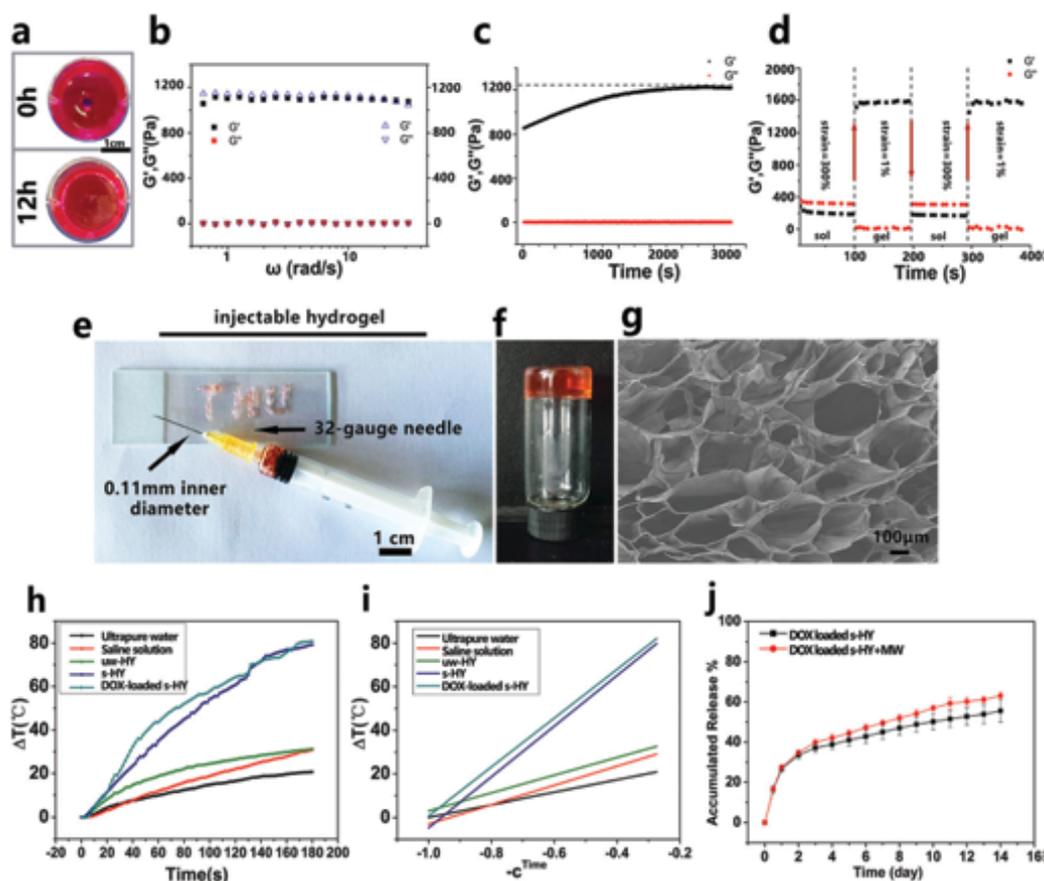
Fig. 2 Characteristics of the injectable ionic hydrogel. (a) Appearance of the self-healing ionic hydrogel *versus* time. The hydrogel was stained with rhodamine B for observation. (b) Storage modulus G' and loss modulus G'' *versus* frequency change before the hydrogel was cut into 4 pieces (left) and after the self-healing process (right). (c) G' and G'' *versus* time during the hydrogel healing process. (d) The damage–healing property of the hydrogel determined by the periodic strain (strain 300–strain 1%) measurements. (e) Digital photograph of the injectable hydrogel indicating that it can pass through a 32-gauge (110 μm) needle without clogging. (f) Stability of the injectable ionic hydrogel for two weeks. (g) The interconnected porous microstructures of the injectable ionic hydrogel obtained by SEM imaging. (h) Evaluation of the microwave susceptible properties of the as-prepared ionic injectable hydrogel. Heating curves of 1 mL hydrogel and 1 mL solution with different formulations under microwave exposure (2 W, 5 min). (i) Fitting curves based on the heating curves in (d). The slope represents the microwave susceptible efficiency of samples, *c* is a constant with a value of 0.99283. (j) Doxorubicin release profile. The promoted group was exposed to 2 W microwave radiation for 5 minutes every 48 hours. Data are shown as the mean ± standard error.

4112 | *J. Mater. Chem. B*, 2017, 5, 4110–4120

This journal is © The Royal Society of Chemistry 2017

1% at the same frequency (1 Hz) was applied (Fig. 2d). The G' of the self-healing hydrogel sharply decreased from about 1500 Pa to 200 Pa at a large dynamic strain (300%) which induced a gel-to-sol transition. At the lower strain (1%), G' quickly returned to the initial value which demonstrated that the ionic hydrogel underwent a rapid sol-to-gel transition. This transition revealed that the uncoupling and recoupling process of the imine linkages in the ionic hydrogel was rather rapid and dynamic, which endowed the hydrogel with excellent injectability (Fig. 2e). Fig. 2f demonstrates that the as-prepared DOX-loaded s-HY has excellent spatial stability, which prevents the hydrogel from leaking into the neighboring tissues. The SEM image of the freeze-dried hydrogel in Fig. 2g shows its porous structures with interconnected micropores ranging from 10 to 200 μm (Fig. 1g). The high porosity maintains a rather high loading of ions. As calculated, the saline solution content percentage was up to 97.5%. Since ions encapsulated in microspheres have been reported to induce a higher temperature rise compared to the saline solution under microwave exposure,[9] the porous structure of the ionic hydrogels was supposed to be able to render a similar effect. That is, a strong ion confinement effect could be realized.[36,50]

To verify this conjecture, an *in vitro* microwave heating test was performed to investigate the response properties of the hydrogels to microwave exposure. As shown in Fig. 2h, the most remarkable temperature increase did happen to DOX-loaded s-HY, as it can be noticed that a rather high temperature (~80 °C) can be reached when the hydrogel was exposed to microwave irradiation (2 W, 2.45 GHz) for only 3 min. It has been investigated that the time required to achieve irreversible damage decreases exponentially at temperatures above 60 °C.[51] Therefore, the excellent heating efficiency of DOX-loaded s-HY makes it possible to meet the demand of temperature over 50 °C throughout the entire target for further *in vivo* anti-tumor investigation.[4] It is also worth noting that all the hydrogel formulations can induce a higher temperature increase as compared with solutions with the same composition due to their notable porous structure. To exhibit the difference of the microwave susceptibility between the samples more clearly, a constant c with a value of 0.99238 was introduced for linear fitting of the heating curves (Fig. 2i).[9] The slope of the lines in Fig. 2i represents the microwave susceptible efficiency of samples, where $\Delta T = a - b \cdot c^{Time}$. It noticeably revealed the excellent microwave heating efficiency of s-HY and DOX-loaded s-HY compared with ultrapure water, saline solution and UW-HY, and also with some other reported agents such as microcapsules or ionic liquids.[9,10,31,32] The rapid temperature rise of DOX-loaded s-HY can be expected to reduce the damage of surrounding normal tissues during the microwave treating process *in vivo*. The slight difference in temperature rise between s-HY and DOX-loaded s-HY could be owing to the small amount of ionization by DOX in the hydrogel, which could contribute more friction heat under microwave exposure.

Fig. 2j shows the DOX release profiles of DOX-loaded s-HY under 5 min microwave exposure every 48 h at 37 °C. In the initial 12 hours, both the control group and the ionic hydrogel exposed under microwave exposure group exhibit a rapid drug release speed, releasing around 16.5% DOX. During the next 13 release periods, both groups experienced a stable release. The sustained and stable drug release profile of DOX-loaded s-HY demonstrated its potential in clinical settings. Moreover, the group exposed under microwave shows a slightly increased release (63% during the whole release period) compared to the control group (55%). This may be due to the slight temperature rise in the hydrogel during the microwave exposure process.

In vitro cytotoxicity and *in vivo* biocompatibility and spatial stability of the ionic hydrogel

One of the prerequisites for a microwave susceptible agent is its nontoxicity both *in vitro* and *in vivo*.[52,53] Combining the Live/Dead staining with DNA assay, the cytotoxicity of the ionic hydrogel *in vitro* can be demonstrated. Fig. 3a shows the results of the Live/Dead assay. The hydrolysis of calcein–AM in live cells produces green fluorescence, while propidium iodide can enter into dead cells' DNA double strands and produce red fluorescence. After both 24 h and 72 h incubation, there were almost no dead cells (Fig. 3a). Moreover, it can be seen from Fig. 3b that L929 cells in the hydrogels could maintain a very fast proliferation rate during the whole culture duration. The amount of cells was over 17 times more than the initial cell number after 4 days. The increase of cell number with culture time was significant ($p < 0.05$). These results indicated that s-HY exhibited no obvious cytotoxicity *in vitro*.

As shown by the results of *in vivo* biocompatibility investigation, the presence of neutrophils was noticed in the proximity of the ionic hydrogel samples, indicating a moderate acute inflammatory response at one week post-implantation (Fig. 3c). The foreign body reaction consisted of a few macrophages eroding the surface of the s-HY implant. At four weeks post-implantation (Fig. 3d), this acute inflammatory response turned to be relatively slight as almost no macrophages can be observed. Some of the implanted hydrogels were still present and remained intact in the original position, indicating the spatial stability of the hydrogels *in vivo*. Overall, the implanted hydrogels demonstrated a mild foreign-body reaction indicating their nice biocompatibility, which is one of the most important characteristics of microwave agents for clinical use.[54] The spatial stability of the hydrogels *in vivo* ensured success for repeated microwave therapy processes.

Susceptibility of the ionic hydrogel in a tissue-equivalent phantom model

To evaluate the susceptibility of the ionic hydrogel, a tissue-equivalent phantom model was built with chicken breast. Fig. 4a represents a schematic device that contains the chicken breast. As illustrated in Fig. 4b, 1 mL of ionic hydrogel was injected into the chicken breast, while a microwave antenna was inserted into the center of the ionic hydrogel under a power of 2 W, 2.45 GHz. Three optical fibers were inserted into the center of the ionic hydrogel, in the chicken breast 2 mm away from the hydrogel boundary and in the surrounding water, respectively. Accordingly, the side view and top view pictures of the experimental installation are shown in Fig. 4c and d. As shown in Fig. 4e, the temperature rise in the ionic hydrogel was

This journal is © The Royal Society of Chemistry 2017

J. Mater. Chem. B, 2017, 5, 4110–4120 | 4113
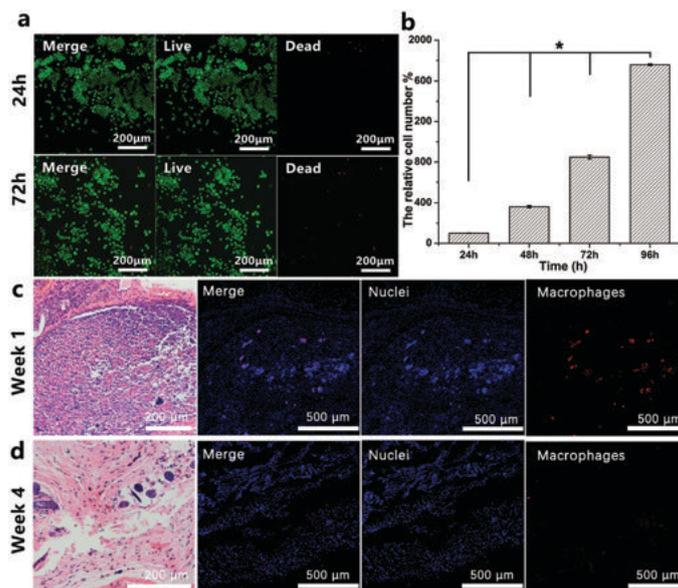
Fig. 3 Hydrogel cytotoxicity *in vitro* and hydrogel biocompatibility and spatial stability *in vivo*: (a) qualitative results obtained using a Live/Dead staining method. (b) Quantitative results obtained by DNA assay ($n = 5$). Live cells were stained green by calcein–AM and dead cells were stained red by propidium iodide. *: $p < 0.05$. (c) H&E staining and immunohistochemical staining results of the s-HY sample and surrounding tissues obtained after one week implantation. (d) H&E staining and immunohistochemical staining results of the s-HY sample and surrounding tissues obtained after four weeks implantation. (The red staining represents the macrophages and blue staining represents the cell nuclei in immunohistochemical photos.)
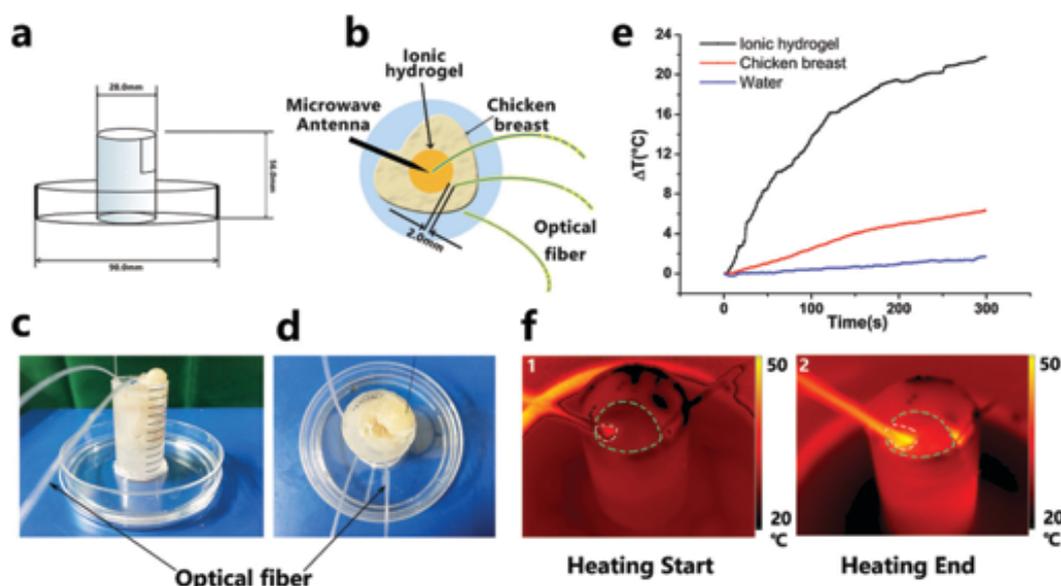
Fig. 4 Realistic scenario simulation experiment. (a) Diagram of the chicken breast container. (b) Diagram of the experimental design. (c) Side view and (d) top view of the experimental installation. (e) Heating curves of the ionic hydrogel, chicken breast and surrounding water under microwave exposure (2 W, 2.45 GHz), respectively. (f) Infrared thermal pictures recorded during the test process. 1 and 2 were captured at the beginning and end of the heating process, respectively. The ionic hydrogel and chicken breast are outlined by white and viridis dotted lines, respectively.

remarkably higher (approximately 4 times) than that in the chicken breast, while the temperature in the surrounding water was almost unchanged. Real-time thermal imaging was performed by using a thermal imager (Ti125, Fluke, America). It also demonstrated that there is a high temperature increase around the hydrogel under 2 W microwave exposure within 5 minutes, and the temperature within the ionic hydrogel marked by the white dotted line was visibly higher than that in the chicken breast marked by the viridis dotted line (Fig. 4f). This indicated that the ionic hydrogel exhibits high susceptibility to microwave irradiation under an ultralow power (2 W, 2.45 GHz), so it may enhance the efficiency of

4114 | *J. Mater. Chem. B,* 2017, **5**, 4110–4120

This journal is © The Royal Society of Chemistry 2017

microwave ablation as well as protect the healthy tissues from overheating.

In vivo microwave tumor ablation therapy

The anti-tumor investigation of the ionic hydrogel showed that the microwave exposure could induce a remarkably higher temperature rise and a wider high temperature range in tumors for the DOX-HY + MW group, compared with the MW and control groups (Fig. 5a). The surface temperature in the tumor area was up to 50 °C in the DOX-HY + MW group (Fig. 5a). This indicated that DOX-loaded s-HY demonstrated excellent treatment efficiency as a microwave susceptible agent *in vivo*. After being treated for 14 days, neither the microwave exposure alone nor DOX-HY alone could affect the tumor growth compared with the control group, as shown in Fig. 5b. In contrast, the mice that were treated with DOX-HY + MW demonstrated a significantly effective suppression of tumor growth within 2 weeks. There is a slight

decrease in the tumor volume of the DOX-HY + MW group compared with that of the HY + MW group, which is thought to be the result of the combination of microwave ablation and chemotherapy using a small amount of DOX in the hydrogel. The black scars on the skin at the tumor site in the DOX-HY + MW group (Fig. 5c) indicated the stability of the hydrogels implanted into the tumor, which led to the success of the microwave ablation treatments.[37] H&E staining of tumors in the DOX-HY + MW group showed much fewer cells than the control group (Fig. 5d), indicating that thermal therapy by DOX-HY + MW had a significant suppression of tumor growth.

The macrobiological toxicity of the ablation treatment was evaluated by measuring the variation in mice body weight. As shown in Fig. 5e, there was no significant difference between the experiment groups and control group (Fig. 5e). A histological study on organs (including heart, liver, spleen, lungs and kidneys) showed that no obvious change could be observed in the
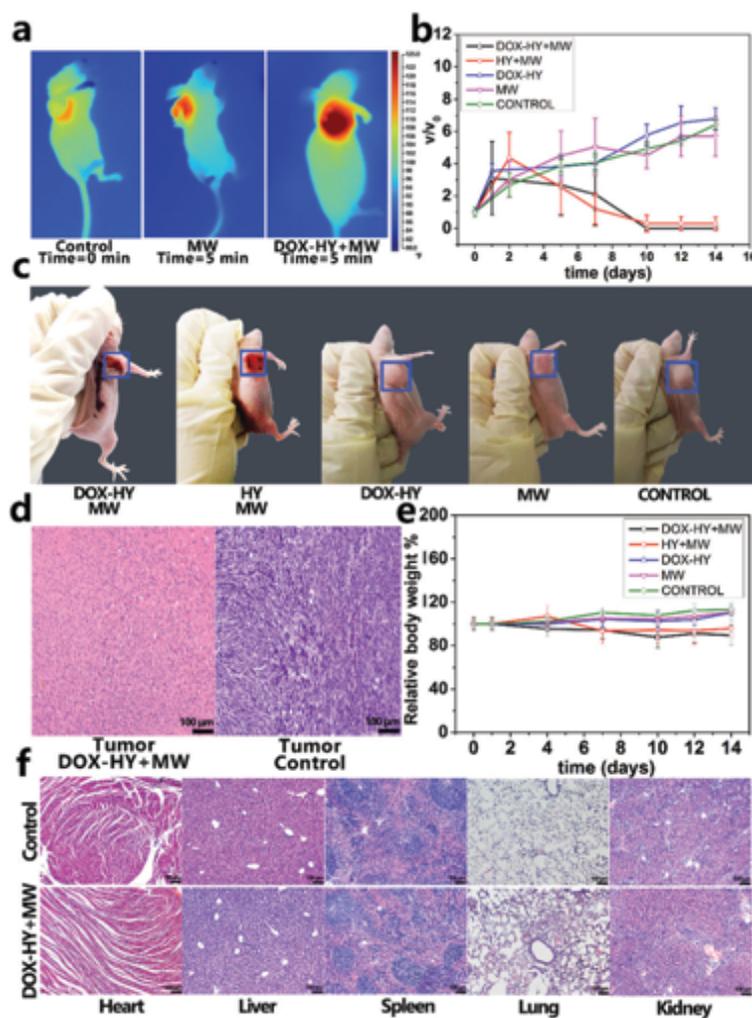
Fig. 5 Evaluation of the ionic hydrogel microwave ablation treatment efficiency *in vivo*. (a) Infrared thermal photographs of nude mice, DOX-HY + MW group and only MW group, respectively. (b) Relative tumor volume change with SHG-44 tumors under various treatments (*n* = 5). (c) Photographs of nude mice after 14 days microwave treatment in the DOX-HY + MW, HY + MW, DOX-HY, MW, CONTROL groups, respectively. (d) H&E staining results of tumors after DOX-HY + MW therapy compared to that of the control group. (e) Relative body weight of nude mice under different treatments (*n* = 5), data are presented as relative mean ± SD. (f) Histological section of tissues (heart, liver, spleen, lungs and kidneys) obtained from nude mice in the DOX-HY + MW and control groups after 14 days therapy.

This journal is © The Royal Society of Chemistry 2017

J. Mater. Chem. B, 2017, 5, 4110–4120 | 4115

DOX-HY + MW group compared with the control group (Fig. 5f). These results indicated that the treatment by microwave exposure using DOX-loaded s-HY as the susceptible agent had no apparent toxic side-effects on the mice throughout the whole study period.

Mechanisms of microwave-based cell death

In light of the temperature range in thermal therapy, normally mild hyperthermia (heating temperature ranges at 40–45 °C) has been able to cause irreversible cell damage. In this temperature range, however, only after a prolonged exposure time (from 30 to 60 minutes) such irreversible cell damage will occur,[55] and because of continued cellular functioning as well as tumor recurrence even prolonged exposure will not kill all the cancer cells.[4,56] In contrast, microwave ablation (heating temperature > 60 °C)[3] is considered to kill cells by the mechanisms of direct hyperthermic injury which can immediately lead to coagulative necrosis.[51] The direct cellular damage caused by microwave exposure mainly occurs in three ways from the subcellular level to the tissue level. As shown in Fig. 6, the change in cell membrane integrity was considered as the main cause of hyperthermia-induced cell death.[57] In addition, intracellular mitochondrial dysfunction was reported to have a close relationship with direct heat-induced injury. It has been demonstrated that the ablation temperature could promote proton leakage from the inner mitochondrial membrane.[58] Moreover, hyperthermia can rapidly inhibit DNA replication during cell division.[59] It is well known that uncontrolled cell proliferation is a significant hallmark of cancer. That is, the heat inhibition of DNA replication suggests heat-mediated reproductive cell death.[59] Overall, all these intracellular damages result in rapid protein denaturation and direct cell death. Therefore, microwave ablation could utilize high temperature to induce focal hyperthermic intracellular injury and ultimately tumor coagulative necrosis. Based on the above observation, our work successfully combined direct intracellular damage by microwave ablation with the susceptibility of the ionic hydrogel and then realized excellent therapeutic efficiency *in vivo*.

Microwave temperature rise mechanism *via* computer simulation

For a microwave heating mechanism, the qualitative explanation was that an electric field will induce ionic polarization and cause the temperature rise. But there were no quantitative data about
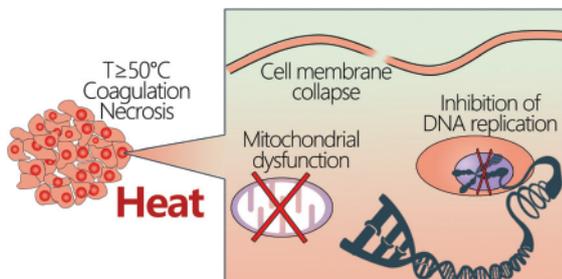
Fig. 6 The hyperthermia zone exhibits coagulative necrosis at temperatures ≥50 °C and direct cell damage induced by hyperthermia including cell membrane collapse, mitochondrial dysfunction and inhibition of intracellular DNA replication.

the difference between hydrogels and saline solution when exposed to microwave radiation. To systematically investigate the interaction between microwave radiation and hydrogels, computer simulation was applied to the saline solution and s-HY, respectively.

An *in vitro* experimental model consisting of a tube and a microwave emission source was built by using Catia v56r2016 (Fig. 7a). The radius of the tube is 10 mm and the height is 60 mm. The microwave emission source of 1 mm radius was set to be located on the axis of the tube with a distance of 20 mm from the bottom of the tube. The commercially available COMSOL 4.3b software was applied as the simulation platform. With the stipulated excitation at the spherical port, eqn (1) was put forward for the electric field vector E inside the waveguide. And the heat transfer model was applied using the "Heat transfer in Solids" physics module included in COMSOL described as eqn (2).

$$\nabla \times \left(\mu_r^{-1} \times E \right) - k_0^2 \left(\varepsilon_r - \frac{j\sigma}{\omega \varepsilon_0} \right) E = 0 \quad (1)$$

$$\rho C_P \frac{\partial T}{\partial t} + \rho C_P u \cdot \nabla T = \nabla \cdot (k \nabla T) + Q \quad (2)$$

where μ_r represents the relative permeability, j is the imaginary unit, σ is the conductivity, ω represents the angular frequency, ε_r is the relative permittivity, and ε_0 is the permittivity of free space in eqn (1), and ρ is density of solution, C_P is the specific heat of solution, k is the heat conductivity coefficient, u is the length of the radiation path, and Q represents heat source in eqn (2).

The permittivity and specific heat of the saline solution and s-HY tested by using an S-parameter network analyzer and thermal analysis instrument, respectively, are shown in Table 1, where the specific heat of s-HY and the saline solution was calculated according to Fig. S1 (ESI†). ε' is the imaginary part of the dielectric constant representing the dielectric loss and ability of the material to be polarized by an external electric field. For the saline solution, ε_r is 76.9907–9.5029j, while for s-HY, ε_r has changed to 28.0565–20.3295j. Other parameters are decided by the materials eigen feature.

The final simulation results are shown in Fig. 7. The model containing s-HY had a markedly higher temperature rise compared to that containing saline water during the whole 180 s simulation time (Fig. 7b and c). The temperature in the antenna plane presented a decrease from the antenna center to the edges. Obviously, the highest temperature rise appeared at the antenna center where the temperature of s-HY was up to 375.43 °C which was much higher than that of the saline solution (111.49 °C). It was mainly because that the dielectric loss value of s-HY was much higher than that of the saline solution (Table 1). The real-time temperature distribution was shown as a function of distance and temperature rise (Fig. 7d and e). Each curve represented the temperature from the antenna center to the edge every 2 seconds. In the simulation results, we set 43 °C as the minimum acceptable temperature for thermal therapy. As we look at the marked hyperthermia zone where the temperature was over 43 °C in the real-time temperature distribution of s-HY and the saline solution, respectively (Fig. 7d and e), it can be found that the s-HY model had a larger radius (3.6 cm) than that of the saline solution

4116 | J. Mater. Chem. B, 2017, 5, 4110–4120

This journal is © The Royal Society of Chemistry 2017
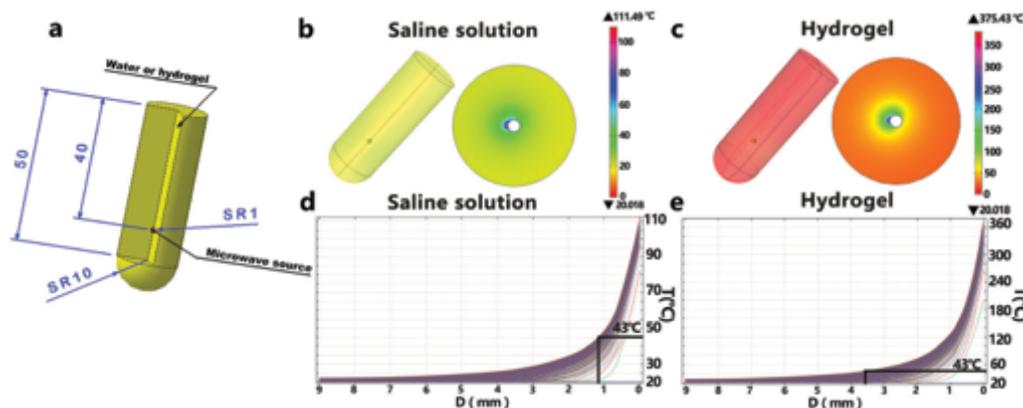
Fig. 7 Computer simulation results of the ionic hydrogel and saline solution. (a) Computer simulation model constructed by using Catia v56r2016. The microwave emission source was inserted into a sphere within the model and its radius was 1 mm. The distance from the bottom to the top of the model was 60 mm, and the distance from the bottom to the microwave source was 20 mm. (b) Microwave heating efficiency and cross section temperature distribution in the saline solution. (c) Microwave heating efficiency and cross section temperature distribution in the ionic hydrogel. (The simulation time was 180 seconds.) (d) Temperature variation of the saline solution from the edge of the model to the center of the microwave source at the source plane. (e) Temperature variation of the ionic hydrogel from the edge of the model to the center of the microwave source at the source plane.

Table 1 The parameters of physical characteristics in saline and the ionic hydrogel

Samples	Relative permittivity ε	Permittivity imaginary part ε'	Specific heat (J g^{-1} °C^{-1})
Saline	76.9907	9.5029	4.11565
Ionic hydrogel	28.0565	20.3295	4.11617

(1.1 cm). These simulation results quantitatively confirmed the experimental results that s-HY could provide a higher temperature rise and a wider high temperature range for microwave thermal therapy. Therefore, a shorter exposure time or a lower microwave power can be expected to induce enough temperature rise and range in the ionic hydrogel for tumor ablation.

Experimental

Materials

Glycol chitosan (CS, 430 kDa) with 75.2% deacetylation was purchased from Wako Pure Chemical Industries Ltd (Tokyo, Japan). The anticancer drug doxorubicin hydrochloride (DOX) was purchased from Tecoland Corporation, USA. Roswell Park Memorial Institute (RPMI) 1640 medium, fetal bovine serum (FBS), calcein acetoxymethyl ester (Calcein–AM), propidium iodide (PI), penicillin–streptomycin (PS) and trypsin were bought from Gibco Life Technologies (Beijing, China). The cell proliferation assay (DNA assay) kit was purchased from Invitrogen Corporation, USA. All materials were used without further purification. SHG-44 cells and L929 cells were obtained from American type culture collection (ATCC).

Preparation of DOX-loaded ionic and ultrapure water hydrogels

Telechelic difunctional poly (ethylene glycol) (DF-PEG) was synthesized by esterification of hydroxyl terminated PEG with 4-formylbenzoic acid.[40] The ionic CS hydrogel (denoted as s-HY) could be formed by blending 3 wt% CS saline solution and 2 wt% DF-PEG saline solution at room temperature in less than 1 min, while the ultrapure water CS hydrogel (denoted as uw-HY) could be formed by mixing ultrapure water solutions of CS and DF-PEG. The volume ratio of CS and DF-PEG solutions in both samples was 1:1. The DOX-loaded hydrogel was simply synthesized by adding DOX (200 μL mL^{-1}) into the DF-PEG solution before blending with the CS solution.

Characterization of the ionic hydrogel

The morphology, permittivity and specific heat of the injectable ionic hydrogel were measured in this work. A scanning electron microscope (SEM MERLIN, ZEISS, Germany) was used to characterize the morphology of the freeze-dried hydrogel. An S-parameter network analyzer (8720ES, HEWLETT PACKARO) was used to measure the permittivity and a thermal analysis instrument (TA instrument, Q2000, America) was utilized to obtain the specific heat of the hydrogel. The heating property of the ionic hydrogel was measured by using a microwave generator (WB-3100AI, Baoxing, China).

The water content of the hydrogel was calculated using eqn (3):

$$\text{Water content}\,(\%) = 100 - \frac{R_{CS}Q_{CS} + R_{PEG}Q_{PEG}}{Q_{CS} + Q_{PEG}} \times 100 \quad (3)$$

where R_{CS} and R_{PEG} represent the ratio of CS and PEG solutions, respectively, and Q_{CS} and Q_{PEG} are the weight of the CS and PEG solutions, respectively.

Self-healing experiments

A hole was punched in the middle of one piece of hydrogel stained with rhodamine B, and photographs at different time intervals were taken to record the self-healing appearance of the hydrogel. Rheology analyses were carried out to quantitatively monitor the self-healing process. To be more specific, the ionic hydrogel (400 μL) was prepared on the parallel plate of the rheometer. After complete gelation, a frequency-dependent

rheological test was carried out to evaluate the storage modulus (G') and loss modulus (G'') of the hydrogel. Then, the hydrogel was cut into 4 pieces to real-time monitor the self-healing process. The G' and G'' values of the broken hydrogel versus time were recorded. Subsequently, the same frequency-dependent rheological test was carried out to compare the mechanical characteristics of the healing hydrogel with that before cutting. In addition, the G' and G'' values versus shear stress were recorded to evaluate the strain-induced damage and to test the recovery mechanical properties of the ionic hydrogel. The strain amplitude changed from maximum 300% to minimum 1% at the same frequency (1.0 Hz), and the process was repeated twice.

Microwave heating experiments

To evaluate the microwave susceptible properties of the as-prepared hydrogels, an in vitro microwave heating experiment was carried out. 1 mL hydrogels of different formulations, including DOX-loaded s-HY, s-HY, and uw-HY were exposed to microwave radiation through a microwave antenna (0.88 mm in diameter and 15.8 cm in length) for 3 min. 1 mL solutions of the same formulations were employed as controls under the same conditions. During the heating process, the real-time temperature in the hydrogels was monitored and recorded by using an optical fiber every 2 seconds.

In vitro drug release

DOX-loaded s-HY (2 mL) was placed into 5 mL PBS solution, and was incubated in a 37 °C water bath. The hydrogel with PBS solution was exposed to microwave radiation (2 W, 2.45 GHz) for 3 min every 48 hours to accelerate drug release. The whole process lasted for two weeks. After a designated period of time, 5 mL of incubated solutions were collected to test the DOX release. The control group contained samples incubated under same conditions without microwave exposure. The amount of DOX released was determined by measuring the ultraviolet absorbance of DOX. A standard absorbance curve of DOX was measured beforehand. The final accumulated amount of DOX released from the experimental group and the control group was calculated by adding up the DOX content of every test. Each group contained five parallel samples.

Cell culture, in vitro cytotoxicity evaluation

L929 cells ($\sim 10^4$ cells per well, 48-well plates) were cultured on s-HY and maintained in Roswell Park Memorial Institute (RPMI) 1640 medium with 10% FBS and 1% PS in a humid atmosphere with 5% CO_2 for 4 days to investigate the in vitro cytotoxicity of the hydrogel through cell proliferation. The cell culture medium was replaced every two days. Live/Dead staining was conducted after the cells were incubated for 24 h and 72 h to qualitatively evaluate the cell viability. Calcein–AM and propidium iodide were used to stain live and dead cells, respectively. The fluorescence was determined with excitation at 490 nm by using a confocal laser scanning microscope (CLSM, TCS SP5, Leica Microsystem, Germany). Moreover, the cell number was measured using a Hoechst DNA assay to investigate cell proliferation. 500 μL per well CyQUANT GR dye working solution (Invitrogen)

was added into the hydrogel with cells every 24 h. The fluorescence of the system was then calculated by using a microplate reader (EnSpire, Perkin Elmer, America) with excitation at 480 nm and emission at 520 nm. The cell proliferation number was calculated from the fluorescence intensity.

In vivo biocompatibility and spatial stability of the s-HY hydrogel

Animal experiments were performed in compliance with the Institutional Animal Care and Use Committee (IACUC) of Tsinghua University. 6 week-old male ICR mice with an average weight of 16.9 g were anesthetized by pentobarbital sodium (2 wt%, 0.1 mL) and disinfected by medical alcohol before they were implanted subcutaneously with 100 μL injectable s-HY. The two groups of mice were sacrificed after one week and four weeks, respectively. The surrounding tissues were excised and fixed in 4% neutral buffered formalin for further hematoxylin–eosin (H&E) histological analysis and immunohistochemical analysis. In the immunohistochemical analysis, rat anti-mouse CD68 antibody (sc-59103, Santa Cruz Biotechnology, America) was used to identify macrophages around the hydrogel and nuclei were visualized by counterstaining with DAPI.

Susceptibility of the ionic hydrogel in a tissue-equivalent phantom model

To evaluate susceptibility of the ionic hydrogel inside a more realistic physiological environment, a piece of chicken breast saturated in water was used to test the temperature difference between the center of the ionic hydrogel and the outer shell of the tissue. 1 mL of ionic hydrogel was injected into the chicken breast, while a microwave antenna was inserted into the center of the ionic hydrogel under a power of 2 W, 2.45 GHz. Three optical fibers were inserted into in the center of the ionic hydrogel, in the chicken breast 2 mm away from the hydrogel boundary and in the surrounding water, respectively. The temperature rise was real-time monitored during 5 min heating duration. At the beginning and end of the heating process, infrared thermal imaging was performed using a thermal imager (Ti125, Fluke, America).

In vivo microwave thermal therapy

6 week-old male BALB/c nu/nu mice were obtained from IACUC of Tsinghua University. A tumor-bearing mouse model was established by subcutaneous injection of SHG-44 cells (5 × 10^6 cells suspended in 200 μL PBS) into the right flank region of the mice. When the tumors grew up to an average size of 0.26 cm³, the mice were randomly divided into five groups (5 mice each group) and treated under the following conditions: control group, microwave treatment without hydrogels, DOX-loaded s-HY treatment only, microwave treatment with s-HY and microwave treatment with DOX-loaded s-HY. These five groups were marked as CONTROL, MW, DOX-HY, HY + MW, DOX-HY + MW, respectively, and each group contained three mice. For the samples treated with s-HY and DOX-loaded s-HY, 100 μL hydrogel was administered by in situ intra-tumoral injection. A thermal dose of 2 W, 2.45 GHz microwave radiation

4118 | J. Mater. Chem. B, 2017, 5, 4110–4120

This journal is © The Royal Society of Chemistry 2017

by a microwave antenna (0.88 mm in diameter and 15.8 cm in length) was exploited for 5 minutes each time and repeated every two days. All the treated mice were anesthetized by pentobarbital sodium (2 wt%, 0.1 mL) throughout the therapy process. Real-time thermal imaging was performed using a thermal mager (Ti125, Fluke, America). After each therapy process, the tumor volume and body weight were measured and recorded. The tumor volume was calculated using eqn (4):

$$V = \frac{ab^2}{2} \tag{4}$$

where a and b represent the longest and shortest lengths of tumors, respectively.

The mice were sacrificed after a two-week treatment course, and the organs, including liver, spleen, lungs, and kidneys, were excised and fixed in 4% neutral buffered formalin, embedded in paraffin, sectioned, and stained with H&E for the histological study.

Statistical analysis

All results were presented as mean ± standard deviation (SD). Comparisons of the data were carried out using a one-way analysis of variance (ANOVA) followed by the Bonferroni *post hoc* test. Differences were regarded as statistically significant at $p < 0.05$ using Student's t test.

Conclusions

This work presents a first trial on a chitosan based injectable ionic hydrogel with excellent biocompatibility as a microwave susceptible agent. Our observations confirm that the as-synthesized hydrogel has excellent microwave susceptibility properties that can successfully convert microwave radiation into localized heat. Great spatial stability *in situ* ensures success for repeated therapy processes *in vivo*. Besides, the susceptibility of the ionic hydrogel in a tissue-equivalent phantom model indicated that the ionic hydrogel could be significantly heated without any overheating of the surrounding tissue under an ultralow microwave power (2.0 W, 2.45 GHz). The anti-tumor therapy in mice reveals excellent microwave ablation effect enhanced by the ionic hydrogel without any obvious damage, toxicity and side effects. Further computer simulation explained the heating mechanism between microwave radiation and the ionic hydrogel quantitatively. In summary, this simple but novel chitosan-based injectable ionic hydrogel has exhibited huge potential for application in microwave tumor ablation.

Conflict of interest

There are no conflicts of interest to declare.

Acknowledgements

References

1 D. N. Wheatley, C. Kerr and D. W. Gregory, *Int. J. Hyperthermia*, 1989, **5**, 145–162.
2 P. L. Pereira, *Eur. J. Radiol.*, 2007, **17**, 2062–2070.
3 K. F. Chu and D. E. Dupuy, *Nat. Rev. Cancer*, 2014, **14**, 199–208.
4 S. N. Goldberg, G. S. Gazelle and P. R. Mueller, *Am. J. Roentgenol.*, 2000, **174**, 323–331.
5 M. G. Lubner, C. L. Brace, J. L. Hinshaw and F. T. Lee, *J. Vasc. Intervent. Radiol.*, 2010, **8**, S192–S203.
6 X. Wang, K. Liu, G. Yang, L. Cheng, L. He, Y. Liu, Y. Li, L. Guo and Z. Liu, *Nanoscale*, 2014, **6**, 9198–9205.
7 T. Liu, C. Wang, W. Cui, H. Gong, C. Liang, X. Shi, Z. Li, B. Sun and Z. Liu, *Nanoscale*, 2014, **6**, 11219–11225.
8 G. Wang, Z. Gao, S. Tang, C. Chen, F. Duan, S. Zhao, S. Lin, Y. Feng, L. Zhou and Y. Qin, *ACS Nano*, 2012, **6**, 11009–11017.
9 H. Shi, T. Liu, C. Fu, L. Li, L. Tan, J. Wang, X. Ren, J. Ren, J. Wang and X. Meng, *Biomaterials*, 2015, **44**, 91–102.
10 Q. Du, C. Fu, J. Tie, T. Liu, L. Li, X. Ren, Z. Huang, H. Liu, F. Tang, L. Li and X. Meng, *Nanoscale*, 2015, **7**, 3147–3154.
11 M. Lu, J. Chen, X. Xie, L. Liu, X. Huang, L. Liang and J. Huang, *Radiology*, 2001, **221**, 167–172.
12 T. Shibata, Y. Iimuro, Y. Yamamoto, Y. Maetani, F. Ametani, K. Itoh and J. Konishi, *Radiology*, 2002, **223**, 331–337.
13 B. Dong, P. Liang, X. Yu, L. Su, D. Yu, Z. Cheng and J. Zhang, *Am. J. Roentgenol.*, 2003, **180**, 1547–1555.
14 P. Liang, B. Dong, X. Yu, D. Yu, Y. Wang, L. Feng and Q. Xiao, *Radiology*, 2005, **235**, 299–307.
15 P. Liang and Y. Wang, *Oncology*, 2007, **72**(suppl 1), 124–131.
16 C. J. Simon, D. E. Dupuy and W. W. Mayo-Smith, *Radiographics*, 2005, **25**, S69–S83.
17 A. S. Wright, L. A. Sampson, T. F. Warner, D. M. Mahvi and J. F. T. Lee, *Radiology*, 2005, **236**, 132–139.
18 Y. Ni, J. Bi, X. Ye, W. Fan, G. Yu, X. Yang, G. Huang, W. Li, J. Wang, X. Han, X. Ni, Z. Wei, M. Han, A. Zheng, M. Meng, G. Xue, L. Zhang and C. Wan, *Medicine*, 2016, **95**, e3998.
19 J. p. Dou, P. Liang and J. Yu, *Abdom. Radiol.*, 2016, **41**, 650–658.
20 C. O. Kappe, *Angew. Chem., Int. Ed.*, 2004, **43**, 6250–6284.
21 C. L. Brace, *Curr. Probl. Diagn. Radiol.*, 2009, **38**, 135–143.
22 P. Lidström, J. Tierney, B. Wathey and J. Westman, *Tetrahedron*, 2001, **45**, 9225–9283.
23 C. Tian, Y. Du, P. Xu, R. Qiang, Y. Wang, D. Ding, J. Xue, J. Ma, H. Zhao and X. Han, *ACS Appl. Mater. Interfaces*, 2015, **7**, 20090–20099.
24 H. Lv, X. Liang, Y. Cheng, H. Zhang, D. Tang, B. Zhang, G. Ji and Y. Du, *ACS Appl. Mater. Interfaces*, 2015, **7**, 4744–4750.
25 C. Hu, Z. Mou, G. Lu, N. Chen, Z. Dong, M. Hu and L. Qu, *Phys. Chem. Chem. Phys.*, 2013, **15**, 13038–13043.

26 T. Zhang, D. Huang, Y. Yang, F. Kang and J. Gu, *Polymer*, 2012, **53**, 6000–6007.

27 Y. Duan, Z. Liu, H. Jing, Y. Zhang and S. Li, *J. Mater. Chem.*, 2012, **22**, 18291–18299.

28 C. Cui, Y. Du, T. Li, X. Zheng, X. Wang, X. Han and P. Xu, *J. Phys. Chem. B*, 2012, **116**, 9523–9531.

29 K. Y. Park, J. H. Han, S. B. Lee and J. W. Yi, *Composites, Part A*, 2011, **42**, 573–578.

30 Y. Li, G. Chen, Q. Li, G. Qiu and X. Liu, *J. Alloys Compd.*, 2011, **509**, 4104–4107.

31 Q. Du, T. Ma, C. Fu, T. Liu, Z. Huang, J. Ren, H. Shao, K. Xu, F. Tang and X. Meng, *ACS Appl. Mater. Interfaces*, 2015, **7**, 13612–13619.

32 H. Shi, M. Niu, L. Tan, T. Liu, H. Shao, C. Fu, X. Ren, T. Ma, J. Ren, L. Li, H. Liu, K. Xu, J. Wang, F. Tang and X. Meng, *Chem. Sci.*, 2015, **6**, 5016–5026.

33 L. Tan, W. Tang, T. Liu, X. Ren, C. Fu, B. Liu, J. Ren and X. Meng, *ACS Appl. Mater. Interfaces*, 2016, **8**, 11237–11245.

34 D. Long, T. Liu, L. Tan, H. Shi, P. Liang, S. Tang, Q. Wu, J. Yu, J. Dou and X. Meng, *ACS Nano*, 2016, **10**, 9516–9528.

35 W. Tang, B. Liu, S. Wang, T. Liu, C. Fu, X. Ren, L. Tan, W. Duan and X. Meng, *RSC Adv.*, 2016, **6**, 32434–32440.

36 D. Long, J. Mao, T. Liu, C. Fu, L. Tan, X. Ren, H. Shi, H. Su, J. Ren and X. Meng, *Nanoscale*, 2016, **8**, 1144–1151.

37 C. W. Hsiao, E. Y. Chuang, H. L. Chen, D. Wan, C. Korupalli, Z. X. Liao, Y. L. Chiu, W. T. Chia, K. J. Lin and H. W. Sung, *Biomaterials*, 2015, **56**, 26–35.

38 C. Wang, X. Wang, K. Dong, J. Luo, Q. Zhang and Y. Cheng, *Biomaterials*, 2016, **104**, 129–137.

39 S. W. Kim, Y. H. Bae and T. Okano, *Pharm. Res.*, 1992, **9**, 283–290.

40 T. C. Tseng, L. Tao, F. Y. Hsieh, Y. Wei, I. M. Chiu and S. h. Hsu, *Adv. Mater.*, 2015, **27**, 3518–3524.

41 B. Yang, Y. Zhang, X. Zhang, L. Tao, S. Li and Y. Wei, *Polym. Chem.*, 2012, **3**, 3235.

42 Y. Zhang, L. Tao, S. Li and Y. Wei, *Biomacromolecules*, 2011, **12**, 2894–2901.

43 Y. Zhang, B. Yang, X. Zhang, L. Xu, L. Tao, S. Li and Y. Wei, *Chem. Commun.*, 2012, **48**, 9305.

44 A. S. Mao, J. W. Shin, S. Utech, H. Wang, O. Uzun, W. Li, M. Cooper, Y. Hu, L. Zhang, D. A. Weitz and D. J. Mooney, *Nat. Mater.*, 2017, **16**, 236–243.

45 K. S. Soppirnath and T. M. Aminabhavi, *Eur. J. Pharm. Biopharm.*, 2002, **1**, 87–98.

46 J. A. Hunt, R. Chen, T. van Veen and N. Bryan, *J. Mater. Chem. B*, 2014, **2**, 5319–5338.

47 P. Wang, W. Chu, X. Zhuo, Y. Zhang, J. Gou, T. Ren, H. He, T. Yin and X. Tang, *J. Mater. Chem. B*, 2017, **5**, 1551–1565.

48 T. Shirakura, T. J. Kelson, A. Ray, A. E. Malyarenko and R. Kopelman, *ACS Macro Lett.*, 2014, **3**, 602–606.

49 B. P. Purcell, D. Lobb, M. B. Charati, S. M. Dorsey, R. J. Wade, K. N. Zellars, H. Doviak, S. Pettaway, C. B. Logdon, J. A. Shuman, P. D. Freels, J. H. Gorman III, R. C. Gorman, F. G. Spinale and J. A. Burdick, *Nat. Mater.*, 2014, **13**, 653–661.

50 X. Li and W. Zhen, *Nanotechnology*, 2011, **22**, 045707.

51 M. Nikfarjam, V. Muralidharan and C. Christophi, *J. Surg. Res.*, 2005, **2**, 208–223.

52 D. F. Williams, *Biomaterials*, 2008, **29**, 2941–2953.

53 J. P. Draye, B. Delaey, A. Van de Voorde, A. Van Den Bulcke, B. De Reu and E. Schacht, *Biomaterials*, 1998, **19**, 1677–1687.

54 K. Y. Lee and D. J. Mooney, *Chem. Rev.*, 2001, **101**, 1869–1880.

55 H. H. Pennes, *J. Appl. Physiol.*, 1998, **85**, 5.

56 M. H. Seegenschmiedt, L. W. Brady and R. Sauer, *Am. J. Clin. Oncol.*, 1990, **4**, 352–363.

57 M. B. Yatvin, *Int. J. Radiat. Biol. Relat. Stud. Phys., Chem. Med.*, 1977, **32**, 513–521.

58 W. T. Willis, M. R. Jackman, M. E. Bizeau, M. J. Pagliassotti and J. R. Hazel, *Am. J. Physiol.: Regul., Integr. Comp. Physiol.*, 2000, **278**, R1240.

59 R. L. Warters, *Radiat. Res.*, 1982, **92**, 458–462.

4120 | *J. Mater. Chem. B*, 2017, **5**, 4110–4120

This journal is © The Royal Society of Chemistry 2017